arXiv:2610.38461v1 [nlin.PS] 28 Oct 2026

Series approximation of discrete-soliton solutions of the DNLS equation

V. Tsiantou,[1] V. Koukouloyannis,[1] K. D. Housiadas,[1] and P.G. Kevrekidis[2]

[1]*Department of Mathematics, University of the Aegean, Karlovasi, 83200 Samos, Greece*
[2]*Department of Mathematics and Statistics, University of Massachusetts, Amherst MA 1003-4515, USA*

We study standing waves of the discrete nonlinear Schrödinger (DNLS) equation by means of perturbative series expansions in the inter-site coupling parameter ε. Power-series approximations are derived for three representative configurations: a single-site soliton and the two two-site ones, namely the in-phase and the out-of-phase configurations. Although higher-order truncations are increasingly accurate for small ε, the expansions possess a small radius of convergence and cease to be useful well before $\varepsilon = \mathcal{O}(1)$. To extend their range of validity we apply the Euler convergence-acceleration method, constructing an optimally transformed series for each lattice site individually. The transformed solution is shown to have substantially better convergence radius and preserves the localization of the solution much better than the original series solution. We then insert the series profiles into the linearization matrix of the DNLS equation in order to obtain improved approximations of the stability eigenvalues, with particular attention to the unstable real eigenvalue of the in-phase configuration. Optimal truncation of the corresponding expansion yields a closed-form $\mathcal{O}(\varepsilon^{5/2})$ estimate, which significantly extends the known $\mathcal{O}(\varepsilon^{1/2})$ leading-order result to considerably larger couplings, while the semi-numerical use of the accelerated profiles reproduces the numerically computed eigenvalue to values of ε of $\mathcal{O}(1)$. Throughout, both the solution profiles and their stability eigenvalues are benchmarked against the numerical solution obtained through a continuation procedure from the anti-continuum limit.

I. INTRODUCTION - THE MODEL

Coherent structures arise ubiquitously in nonlinear dispersive media, where the interplay between dispersion (or discrete diffraction) and nonlinearity supports robust, spatially localized excitations that propagate or remain pinned without dispersing [1]. Such structures — solitons, vortices, kinks and breathers — have been investigated extensively over the past several decades in both continuous and discrete settings, with applications ranging from nonlinear optics and Bose–Einstein condensates (BECs) to biophysics, condensed matter and electrical lattices [1–6]. Discreteness introduces qualitatively new phenomena absent in the continuum limit, most notably the existence of exponentially localized, time-periodic solutions known as discrete breathers [7] or, in the Hamiltonian gauge of the discrete nonlinear Schrödinger (DNLS) equation, discrete solitons in the form of standing waves [5]. It is relevant to point out that such discrete solitonic structures have been extensively studied for multiple decades as evidenced by corresponding reviews [42, 43], they continue to be of current interest to this day. This is, to a significant degree, due to the fact that novel settings manifesting their robust existence continue to emerge, ranging from accordion BEC lattices [39], to optically induced lattices in atomic vapors [44].

The rigorous foundation of the theory of discrete breathers was laid by MacKay and Aubry [7], who proved that, starting from the so-called anti-continuum (AC) —also referred to, early on, as anti-integrable— limit of uncoupled nonlinear oscillators, time-periodic and exponentially localized solutions persist for small values of the coupling parameter under generic non-resonance conditions. This anti-continuum-limit construction has since become a canonical framework for proving the existence of multi-site breathers and discrete solitons in a variety of lattice models, and extensive reviews of the relevant phenomenology can be found in Refs. [8–11]. In the case of the DNLS equation, which is the focus of the present work, the anti-continuum limit corresponds to vanishing inter-site coupling $\varepsilon \to 0$, where the trivial solutions consist of arbitrary superpositions of (without loss of generality) unit-amplitude excitations and empty sites; these solutions can be continued to $\varepsilon > 0$ to yield families of discrete solitons parametrized by ε [5].

Beyond the question of existence, the linear stability of these structures has attracted considerable attention, since stability ultimately determines which configurations are dynamically robust and, hence, the best candidates toward being physically observable. For the one-dimensional DNLS lattice, a systematic stability theory of discrete solitons bifurcating from the anti-continuum limit was developed in the work of [12], who classified the unstable eigenvalues of arbitrary in-phase/anti-phase multi-site configurations and proved that, near $\varepsilon = 0$, the only linearly stable configurations are those formed by alternating anti-phase excited nodes. Companion results for discrete vortices in two-dimensional DNLS lattices were obtained in Ref. [13] with generalizations in three-dimensional settings in [14], and the associated internal modes were analysed in Ref. [15]. Arguably, the most elemental multi-site configuration is that with two excited nodes, which is unstable when they bear the same phase (phase-difference of 0 or in-phase configuration) and spectrally stable near the anti-continuum limit when they bear a phase-difference of π (out-of-phase configuration). The unstable real eigenvalue associated with an in-phase two-site soliton was shown to scale as $\lambda = 2\sqrt{\varepsilon}$ to leading order [12], a result that we will

use as a benchmark below.

It is worth noting in passing a sequence of parallel developments in the realm of genuine discrete breathers (involving infinitely many frequencies via harmonic generation) in Klein-Gordon and Fermi-Pasta-Ulam-Tsingou lattices [9]. In particular, following on the seminal earlier work of [16] and of [11], an alternative approach to the stability of multibreathers in Klein–Gordon chains has been developed in [17]. It has been based on the averaging theory for Hamiltonian systems in action–angle variables originally introduced by MacKay and coworkers [18, 19]. This provides an $\mathcal{O}(\sqrt{\varepsilon})$ estimate of the characteristic Floquet exponents and yields, for soft (hard) on-site nonlinearities, simple criteria determining which sign of the phase difference between adjacent excited sites supports stable multibreather configurations. The equivalence between these two complementary approaches was subsequently established in Ref. [20], and the framework has been extended in several directions, including interactions beyond nearest neighbors [21] and resonances and bifurcations of breathers with holes [22].

A common feature of all the analytical approaches in the vicinity of the AC limit is that they rely on a perturbative expansion of the localized solution, and of its stability eigenvalues, around $\varepsilon = 0$. Such expansions capture the solution accurately for sufficiently small ε, but they lose their predictive power well before ε reaches $\mathcal{O}(1)$, where numerical continuation typically remains perfectly feasible. Direct approximations of DNLS solitons that go beyond the leading-order anti-continuum construction have also been proposed [23]. This raises a natural question: to what extent can one extend the predictive range of the perturbative series, both for the soliton profile itself and for its stability eigenvalues, by means of convergence-acceleration techniques applied to the truncated expansion? Series-acceleration methods — Euler, Borel, Padé, Shanks — have a long history in applied mathematics and asymptotic analysis [24–35], and have been shown to improve dramatically the accuracy of perturbative expansions in a variety of physical contexts; a recent example in the context of viscoelastic flows can be found in Ref. [36].

In the present work we pursue exactly this program for the prototypical example of the cubic DNLS equation. We compute high-order perturbative series for three of the most elemental and representative configurations: a single-site discrete soliton, an in-phase two-site soliton and an out-of-phase two-site soliton. We use the Euler transform to extend the validity range of these expansions. We then feed the accelerated convergence soliton profiles into the linearization (stability) matrix [5] in order to obtain improved estimates of the unstable eigenvalues, which we compare against full numerical continuation of both the soliton profile and its spectrum. As we shall see, this procedure substantially enlarges the parameter range in which the perturbative series faithfully reproduces the numerical result, and it also delivers a compact analytical formula for the stability eigenvalues of the two-site configurations that improves on the known leading-order estimates.

This paper is organized as follows. In Sec. II we briefly present the Euler transformation algorithm, in both its standard and its "improved" form. In Sec. III we derive series approximations for the three discrete-soliton configurations considered and assess their accuracy against numerical continuation. In Sec. IV we use these approximations to compute the stability eigenvalues of the two-site configurations, and we derive improved analytical estimates for them. Finally, Sec. V summarizes our conclusions and outlines directions for future work.

II. THE EULER TRANSFORM

The Euler transformation is a linear method for accelerating the convergence of a (sign-)alternating series. Consider the series

$$\mathcal{S} = \sum_{j=0}^{\infty} (-1)^j \alpha_j = \alpha_0 - \alpha_1 + \alpha_2 - \alpha_3 + \ldots, \quad \alpha_j > 0.$$

Then, the Euler transformation is defined by the series [37]

$$\mathcal{E} = \sum_{j=0}^{\infty} \frac{(-1)^j \Delta^j \alpha_0}{2^{j+1}}, \tag{1}$$

where $\Delta^j \alpha_m$ denotes the forward difference $\Delta^j \alpha_m = \sum_{k=0}^{j} (-1)^k \binom{j}{k} \alpha_{m+j-k}$, and $\binom{j}{k}$ is the binomial coefficient. As has been shown (see e.g. [25] §8), this series can have better convergence properties than $\mathcal{S}$. In our work we are going to apply the transform to truncated series of n terms, denoted by $\mathcal{S}_n$ and $\mathcal{E}_n$ respectively.

It is relevant to note that the Euler series can be rewritten as:

$$\mathcal{E} = \frac{\alpha_0}{2} + \frac{\alpha_0 - \alpha_1}{4} + \frac{\alpha_0 - 2\alpha_1 + \alpha_2}{8} + \cdots . \tag{2}$$

The point of the improvement that this reshuffling induces is that for a reasonably smooth, slowly decreasing sequence α_j, the finite differences $\alpha_0 - \alpha_1, \quad \alpha_0 - 2\alpha_1 + \alpha_2, \quad \ldots$ typically become small, while you also acquire the geometric factors 2^{-j-1}. That is where the acceleration in the series convergence comes from.

In [38] a more practical approach to derive the transformation (1) is presented. In order to demonstrate this approach, we initially consider a truncated series with five terms, $\mathcal{S}_5 = \sum_{j=0}^{4} (-1)^j \alpha_j$, and construct the following triangular table:

$$\begin{array}{ccccccc} A_1 & & & & & & \\ & B_1 & & & & & \\ A_2 & & C_1 & & & & \\ & B_2 & & D_1 & & & \\ A_3 & & C_2 & & E_1 & , & \text{where} \\ & B_3 & & D_2 & & & \\ A_4 & & C_3 & & & & \\ & B_4 & & & & & \\ A_5 & & & & & & \end{array} \qquad \begin{array}{rcl} A_1 &=& \alpha_0 \\ A_2 &=& -\alpha_1 \\ A_3 &=& \alpha_2 \\ A_4 &=& -\alpha_3 \\ A_5 &=& \alpha_4 \end{array} .$$

The elements of the first column are the successive signed terms of $\mathcal{S}_5$, while the entries of the following columns $B_i, C_i, \ldots$ are the mean values of the two preceding elements, i.e. $B_i = (A_{i+1} + A_i)/2$, $C_i = (B_{i+1} + B_i)/2$, and so on. We refer to the elements carrying the same index as a "primary diagonal" of the table, e.g. $(A_1, B_1, C_1, D_1, E_1)$, while the "mirroring" elements with increasing indices form a "secondary diagonal", e.g. $(E_1, D_2, C_3, B_4, A_5)$.

The truncated Euler-transformed series $\mathcal{E}_5$ is obtained by summing the elements of the first primary diagonal and halving the result,

$$\mathcal{E}_5 = \frac{1}{2}\left(A_1 + B_1 + C_1 + D_1 + E_1\right) = \frac{1}{32}\left(31\alpha_0 - 26\alpha_1 + 16\alpha_2 - 6\alpha_3 + \alpha_4\right). \tag{3}$$

The right side of (3) can be extracted either by the algorithm described above or directly by applying (1).

However, according to [38], a more accurate approximating series can be obtained using the same construction. The primary diagonals are examined in sequence, and the first one whose elements are all smaller in magnitude than the corresponding elements of the next secondary diagonal is designated as the "principal diagonal" of the table. The best-converging approximation is then obtained by summing the elements of the A column down to the principal diagonal and adding half the sum of the elements of the principal diagonal itself. We denote this transform by $\mathcal{E}_{5i}^{m}$, where the subscript "i" stands for "improved" and the superscript "m" labels the principal diagonal. For example, if $|C_1| > |B_2|$, the first primary diagonal is not the principal one and the second one is examined; if all of its elements are smaller in magnitude than the corresponding elements of the third primary diagonal, i.e. $|B_2| < |A_3|$, $|C_2| < |B_3|$ and $|D_2| < |C_3|$, then it is the principal diagonal and the fastest-converging approximation is $\mathcal{E}_{5i}^{2} = A_1 + \frac{1}{2}\left(A_2 + B_2 + C_2 + D_2\right)$. Five different approximating series can therefore be constructed for $n = 5$; the corresponding conditions and the associated approximations are summarized in Table I. Note that the improved transform $\mathcal{E}_{5i}^{1}$ coincides with the standard Euler transform $\mathcal{E}_5$, while $\mathcal{E}_{5i}^{5}$ coincides with the original truncated series $\mathcal{S}_5$.

Note that, in some works, just one of the $\mathcal{E}_{5i}^{m}$ transforms is used, to avoid the complexity of the selection rule. For example in [36] the $\mathcal{E}_{5i}^{2}$ is used, since it provides a good balance between accuracy and computational complexity for the problems considered in that work.

III. APPLICATION TO DISCRETE-SOLITON SOLUTIONS

A. Mathematical Setup

Our paradigmatic setting involves the one-dimensional cubic DNLS equation in the form

$$\mathrm{i}\dot{u}_i + \varepsilon\left(u_{i+1} - 2u_i + u_{i-1}\right) + |u_i|^2 u_i = 0, \quad i \in \mathbb{Z}, \tag{4}$$

	Condition		Best approximating series
if	$\lvert B_1\rvert < \lvert A_2\rvert$ and $\lvert C_1\rvert < \lvert B_2\rvert$ and $\lvert D_1\rvert < \lvert C_2\rvert$ and $\lvert E_1\rvert < \lvert D_2\rvert$	$\rightarrow$	$\mathcal{E}^1_{5i} = \mathcal{E}_5 = \frac{1}{2}\left(A_1 + B_1 + C_1 + D_1 + E_1\right)$
else if	$\lvert B_2\rvert < \lvert A_3\rvert$ and $\lvert C_2\rvert < \lvert B_3\rvert$ and $\lvert D_2\rvert < \lvert C_3\rvert$	$\rightarrow$	$\mathcal{E}^2_{5i} = A_1 + \frac{1}{2}\left(A_2 + B_2 + C_2 + D_2\right)$
else if	$\lvert B_3\rvert < \lvert A_4\rvert$ and $\lvert C_3\rvert < \lvert B_4\rvert$	$\rightarrow$	$\mathcal{E}^3_{5i} = A_1 + A_2 + \frac{1}{2}\left(A_3 + B_3 + C_3\right)$
else if	$\lvert B_4\rvert < \lvert A_5\rvert$	$\rightarrow$	$\mathcal{E}^4_{5i} = A_1 + A_2 + A_3 + \frac{1}{2}\left(A_4 + B_4\right)$
	else	$\rightarrow$	$\mathcal{E}^5_{5i} = \mathcal{S}_5 = A_1 + A_2 + A_3 + A_4 + A_5$

TABLE I. Selection rule for the improved Euler transformation, illustrated for a five-term truncation. The conditions are tested in the order shown, and the first one that is satisfied fixes the principal diagonal and hence the approximating series.

where $\mathbb{i}$ denotes the imaginary unit, i the lattice site and ε the inter-site coupling. We look for stationary solutions of the form $u_i(t) = v_i e^{\mathbb{i}\omega t}$, where v_i is time independent. Substituting this ansatz into (4) and applying the scaling transformation $v_i \mapsto \sqrt{\omega}\, v_i$, $\varepsilon \mapsto \varepsilon/\omega$, we obtain the monoparametric algebraic form of the equation,

$$-v_i + \varepsilon\left(v_{i+1} - 2v_i + v_{i-1}\right) + |v_i|^2 v_i = 0, \tag{5}$$

which is the form considered throughout this work.

In order to approximate specific configurations of discrete-soliton solutions of (5), we consider series expansions of the solution of the form

$$v_i = v_i^{(0)} + \varepsilon v_i^{(1)} + \varepsilon^2 v_i^{(2)} + \ldots + \varepsilon^n v_i^{(n)}, \tag{6}$$

where i denotes the lattice site and n the order of the approximation. Inserting this truncated series, for all the sites considered, into (5) yields the truncated-series approximation of the solution for the whole lattice. The aim of this paper is to compute such series approximations for three specific discrete-soliton configurations: the single-site (on-site) configuration and the two two-site ones, known as in-phase and out-of-phase. Since the resulting series are only useful over a small range of ε, we employ convergence-acceleration techniques in order to improve the accuracy of the resulting approximations. Specifically, we use the Euler transform, a linear transformation applicable to sign-alternating series. Having improved the accuracy of the computed profiles, we then use them to sharpen the approximation of the corresponding stability eigenvalues obtained in Ref. [12].

B. Single-site configuration

In order to obtain an approximation of the single-site discrete-soliton solution we consider the following truncated series, one for each site of the lattice,

$$\begin{aligned} v_0 &\simeq 1 + \varepsilon v_0^{(1)} + \varepsilon^2 v_0^{(2)} + \ldots + \varepsilon^n v_0^{(n)}, \\ v_i &\simeq 0 + \varepsilon v_i^{(1)} + \varepsilon^2 v_i^{(2)} + \ldots + \varepsilon^n v_i^{(n)}, \quad \forall i \neq 0. \end{aligned} \tag{7}$$

This choice guarantees that in the AC limit $\varepsilon \to 0$ we recover the trivially localized solution $\{\ldots, 0, 0, 1, 0, 0, \ldots\}$. Substituting an approximation of degree n into Eq. (5) and applying perturbation theory order by order, we obtain the corresponding truncated-series solution of Eq. (5) in powers of ε. We denote the set of these solutions for all the sites of the lattice by S_n. For $n = 5$ we obtain

$$S_5 = \{\ldots, 0, v_5, v_4, v_3, v_2, v_1, v_0, v_1, v_2, v_3, v_4, v_5, 0, \ldots\},$$

with

$$\begin{aligned} v_0 &\simeq 1 + \varepsilon - \frac{3\varepsilon^2}{2} + \frac{7\varepsilon^3}{2} - \frac{85\varepsilon^4}{8} + \frac{287\varepsilon^5}{8} & \qquad v_3 &\simeq \varepsilon^3 - 5\varepsilon^4 + \frac{41\varepsilon^5}{2}, \\ v_1 &\simeq \varepsilon - \varepsilon^2 + \frac{5\varepsilon^3}{2} - \frac{15\varepsilon^4}{2} + \frac{195\varepsilon^5}{8} & \qquad v_4 &\simeq \varepsilon^4 - 7\varepsilon^5, \\ v_2 &\simeq \varepsilon^2 - 3\varepsilon^3 + \frac{19\varepsilon^4}{2} - \frac{63\varepsilon^5}{2} & \qquad v_5 &\simeq \varepsilon^5. \end{aligned} \tag{8}$$

The choice $n = 5$ is dictated by the localization of the solution, which ensures that a few sites around the central one suffice to approximately yet quite accurately describe the discrete soliton. Indeed, the expansion of each site starts one order higher than that of its inner neighbour, which is a direct consequence of the exponential localization of the solution; consequently, the higher the degree of the expansion, the more non-zero sites are generated. In the present case we obtain five non-zero sites on each side of the central one, which is sufficient for an adequate representation of the true solution.

In order to assess the accuracy of these approximations we perform a numerical continuation of the trivially localized configuration with respect to ε. We treat this numerical solution as the ground truth and denote it by N. The step used in the parametric continuation procedure is $\Delta\varepsilon = 0.001$ and the solution was approximated to machine precision. In what follows, the total range of ε considered varies depending on the aspect of the problem we examine each time.

Since all the perturbation expansions derived below are sign-alternating, the Euler transformation provides a natural linear acceleration procedure. In what follows we apply both the standard and the improved Euler transformations. Note that the perturbative solution provides a different number of terms for each site, so that transforms of different length are required ($\mathcal{E}_5, \mathcal{E}_4, \mathcal{E}_3, \ldots$). Although the expansion of v_0 contains six terms, the Euler transform is applied to the $v_0 - 1$ series, i.e., to the terms of $\mathcal{O}(\varepsilon)$ and higher orders; in this way, the sequence fed to the transform is strictly alternating and effectively has five terms. Then it is added to the constant term 1 to get the transformed expression for v_0. We denote the set of all these transformed solutions by E_5, and the corresponding set for the improved transformation by E_{5i}; for a general degree n of approximation the analogous sets are denoted by E_n and E_{ni}. The transformed series obtained for each site and for each range of ε are listed in Appendix A.

Figure 1 shows the profile of the numerically computed discrete soliton N together with the S_5, E_5 and E_{5i} approximations. For low coupling ($\varepsilon = 0.1$) all the series provide a reasonable approximation. For $\varepsilon = 0.3$, the S_5 solution starts to deviate from N and its sign-alternating character becomes visible. Finally, for $\varepsilon = 0.5$ the S_5 solution no longer accurately represents the true solution, while only a small deviation at the edges of the lattice starts to appear in the E_5 and E_{5i} approximations as well.

In order to resolve these deviations more clearly we replot the same profiles on a semilogarithmic scale in Fig. 2. The exponential localization of the solution N is evident in all three panels. The deviations at the edges of the lattice already appear at $\varepsilon = 0.1$: the S_5 expansion of v_5 consists of a single term and, as can be seen in Appendix A, the Euler transformation leaves it unchanged. For $\varepsilon = 0.3$ the loss of the localized character of the S_5 solution is considerably more pronounced, and it begins to appear in the Euler approximations as well, since the approximation of the outermost site is common to all of them. Finally, for $\varepsilon = 0.5$ the loss of localization propagates to the inner sites of the E_5 and E_{5i} approximations. Note that, to the naked eye, E_5 and E_{5i} are indistinguishable, so that a more quantitative diagnostic is needed to discern between the two.

In order to quantify the deviation of the approximate solutions from the numerical one, we introduce the relative ℓ_∞ error

$$\epsilon_{S_i} = 100\,\frac{\|S_i - N\|_\infty}{\|N\|_\infty}, \tag{9}$$

expressed as a percentage; the errors ϵ_{E_5} and $\epsilon_{E_{5i}}$ associated with the E_5 and E_{5i} approximations are defined analogously. Figure 3 compares ϵ_{S_5}, ϵ_{E_5} and $\epsilon_{E_{5i}}$. The improved Euler approximation yields the smallest error among all the approximations considered: for small ε it reproduces the error of the fifth-order series S_5, whereas for larger ε it follows

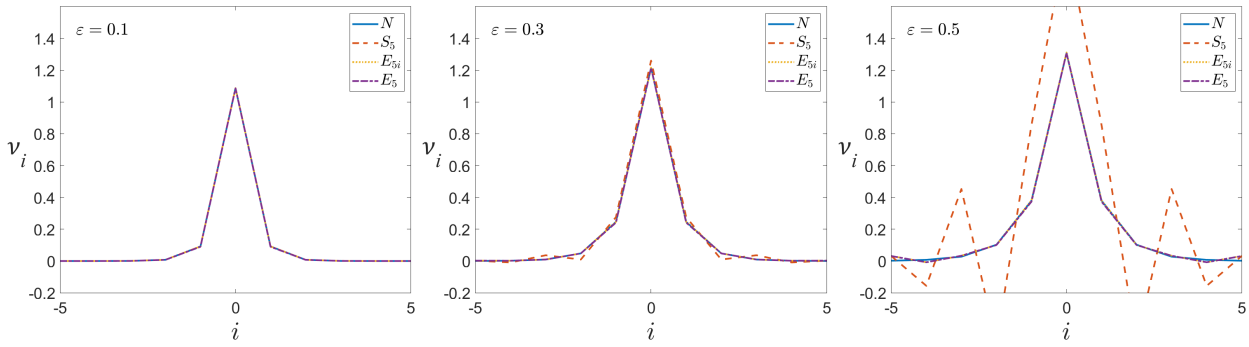


FIG. 1. Profile of the single-site discrete-soliton solution on a linear scale, for three characteristic values of the coupling parameter, namely $\varepsilon = 0.1, 0.3, 0.5$. The numerical solution N (blue, solid) is compared with the standard $n = 5$ term series expansion S_5 (red, dashed), the Euler transform result E_5 (purple, dash-dotted) and the improved variant the latter E_{5i} (yellow, dotted).

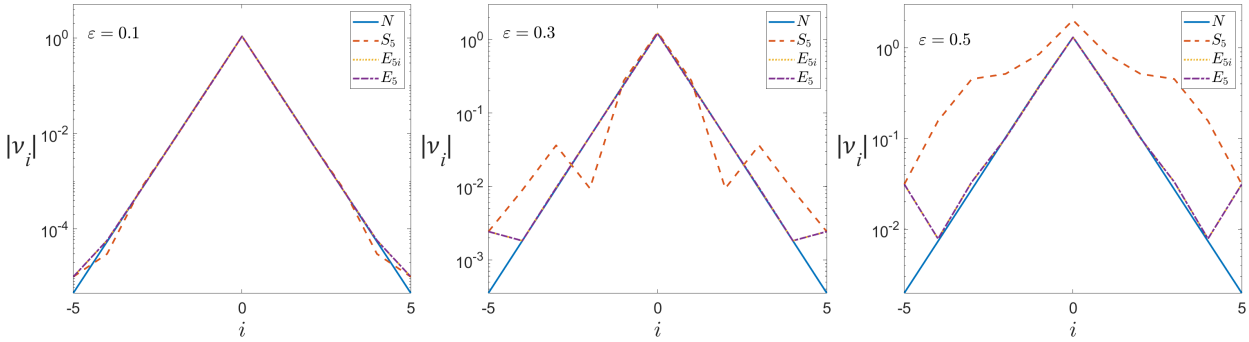


FIG. 2. Profile of the single-site discrete-soliton solution on a semilogarithmic scale, for three characteristic values of the coupling parameter, namely $\varepsilon = 0.1, 0.3, 0.5$. The numerical solution N (blue, solid) is compared with the standard $n = 5$ term series expansion S_5 (red, dashed), the Euler transform result $\mathcal{E}_5$ (purple, dash-dotted) and the improved variant the latter $\mathcal{E}_{5i}$ (yellow, dotted).

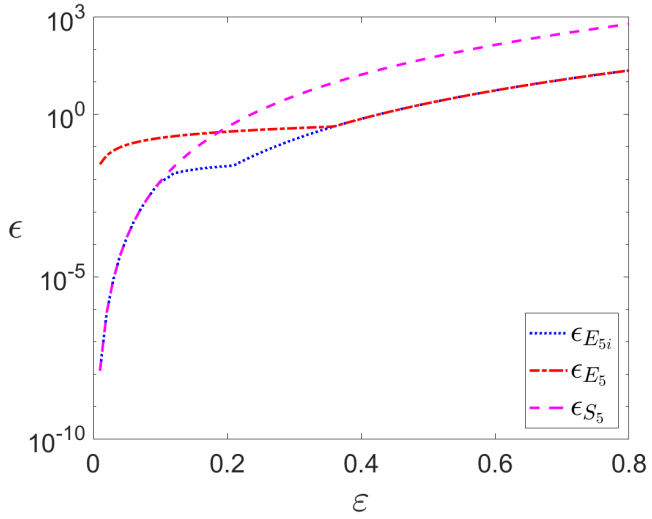


FIG. 3. Absolute relative errors, $\epsilon_{E_{5i}}$ (blue, dotted) of the improved Euler E_{5i}, ϵ_{E_5} (red,dash-dotted) of the Euler E_5 and ϵ_{S_5} (magenta, dashed) of the standard series S_5 as percentages of the approximate solutions on a semilogarithmic scale, for the single-site configuration. The improved Euler approximation consistently exhibits the smallest error with respect to the numerical solution over the range of ε considered.

that of E_5. In other words, the selection rule of Table I automatically switches between the two limiting behaviours, so that the improved Euler transformation provides the closest agreement with the numerical solution over the entire range of ε considered. This mechanism will, in fact, be found to recur in the two remaining configurations.

This behavior reveals that, for small enough values of ε, the most accurate series is the standard S_5 one, while the power of the Euler transformation is revealed for larger values of ε. Thus, as a general remark we could say that, if someone wants the most refined approximation of the solution, he should use the improved Euler transformation. But this comes with the cost of a more complex algorithm. In order to avoid these complications, he can use the standard series for values up to $\varepsilon \leq 0.2$ and switch to the standard Euler transformation for higer values of ε. This improves significantly the convergence of the solution providing an error of $\approx 1\%$ for values of ε up to 0.5 which is adequate for most uses.

C. Two-site configuration: the in-phase case

To obtain the series approximation of the in-phase two-site configuration we again consider an expansion of degree n of the form (6), now for the configuration

$$S_n = \{\ldots, v_2, v_1, v_0, v_0, v_1, v_2, \ldots\},$$

so that in the anti-continuum limit we recover the trivially localized configuration $\{\ldots, 0, 0, 1, 1, 0, 0, \ldots\}$. Inserting this approximation into (5) and applying order-by-order perturbation theory, we obtain, for $n = 5$,

$$\begin{aligned} v_0 &\simeq 1 + \frac{\varepsilon}{2} - \frac{5\varepsilon^2}{8} + \frac{21\varepsilon^3}{16} - \frac{493\varepsilon^4}{128} + \frac{3391\varepsilon^5}{256} & v_3 &\simeq \varepsilon^3 - \frac{11\varepsilon^4}{2} + \frac{195\varepsilon^5}{8}, \\ v_1 &\simeq \varepsilon - \frac{3\varepsilon^2}{2} + \frac{35\varepsilon^3}{8} - \frac{247\varepsilon^4}{16} + \frac{7587\varepsilon^5}{128} & v_4 &\simeq \varepsilon^4 - \frac{15\varepsilon^5}{2}, \\ v_2 &\simeq \varepsilon^2 - \frac{7\varepsilon^3}{2} + \frac{99\varepsilon^4}{8} - \frac{731\varepsilon^5}{16} & v_5 &\simeq \varepsilon^5. \end{aligned} \tag{10}$$

Applying the standard and the improved Euler transformations to S_5 yields the expansions which are listed in the document that supplements this manuscript.

Figure 4 shows the profile of the numerically computed discrete soliton N together with the S_5, E_5 and E_{5i} approximations for the in-phase case. In this configuration we have two central oscillators and the left part of the lattice moves in-phase with its right one, i.e., the configuration preserves the parity symmetry throughout the relevant parametric continuation (as it is a property of the original DNLS model). The situation described in Figure 4 is quite similar to what we observed in the single-site configuration. For low coupling ($\varepsilon = 0.1$) all the series provide a good approximation. For larger values of ε, the Euler approximations still provide a good approximation while the original series becomes quantitatively irrelevant.

In the semilogarithmic version of the profiles (Fig. 5), the deviations at the edges of the lattice are already discernible at small values of ε, while for larger values of ε we can observe the loss of the localization of the S_5 solution. On the other hand, for large values of ε, while it is obvious that the S_5 solution is now highly inaccurate, we can also observe that also the delocalization of the E_5 and E_{5i} solutions becomes gradually evident.

The accuracy of the resulting approximations, measured by the percentage of the absolute relative error of Eq. (9), is shown in Fig. 6. The behavior is the same as in the single-site case: the improved Euler approximation tracks S_5 at small ε and E_5 at large ε, and therefore remains the most accurate of the three throughout the relevant continuation.

D. Two-site configuration: the out-of-phase case

For the out-of-phase two-site configuration we consider the same expansion (6) applied to

$$S_n = \{\ldots, +v_2, +v_1, +v_0, -v_0, -v_1, -v_2, \ldots\},$$

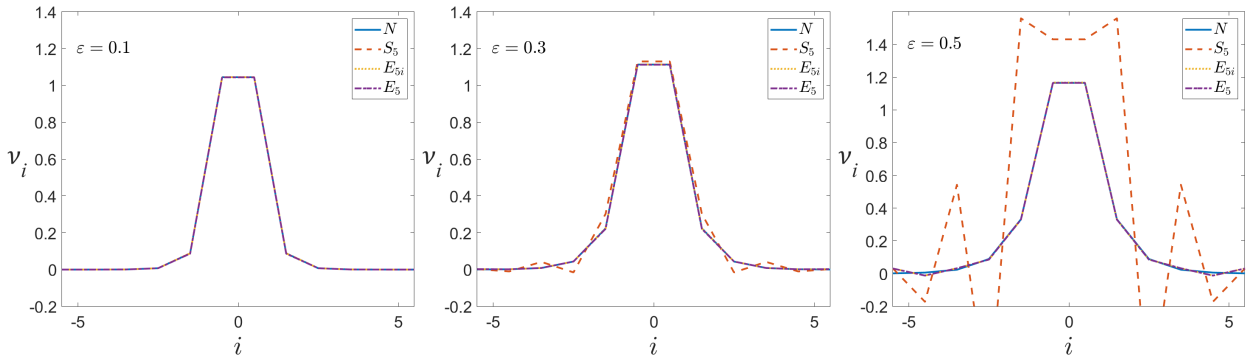


FIG. 4. Profile of the in-phase discrete-soliton solution on a linear scale, for three values of the coupling parameter, namely $\varepsilon = 0.1, 0.3, 0.5$. The numerical solution N (blue, solid) is compared with the standard $n = 5$ term series expansion S_5 (red, dashed), the Euler transform result E_5 (purple, dash-dotted) and the improved variant the latter E_{5i} (yellow, dotted).

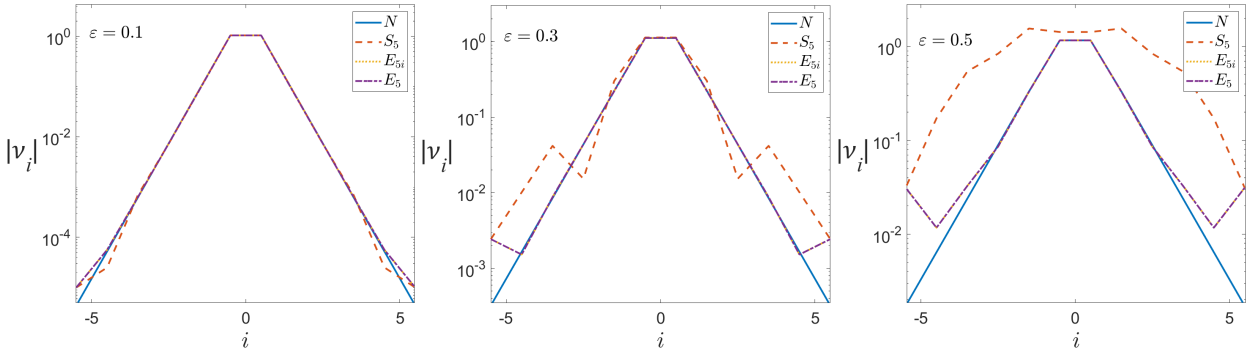


FIG. 5. Profile of the in-phase discrete-soliton solution on a semilogarithmic scale, for three values of the coupling parameter, namely $\varepsilon = 0.1, 0.3, 0.5$. The numerical solution N (blue, solid) is compared with the standard $n = 5$ term series expansion S_5 (red, dashed), the Euler transform result E_5 (purple, dash-dotted) and the improved variant the latter E_{5i} (yellow, dotted).

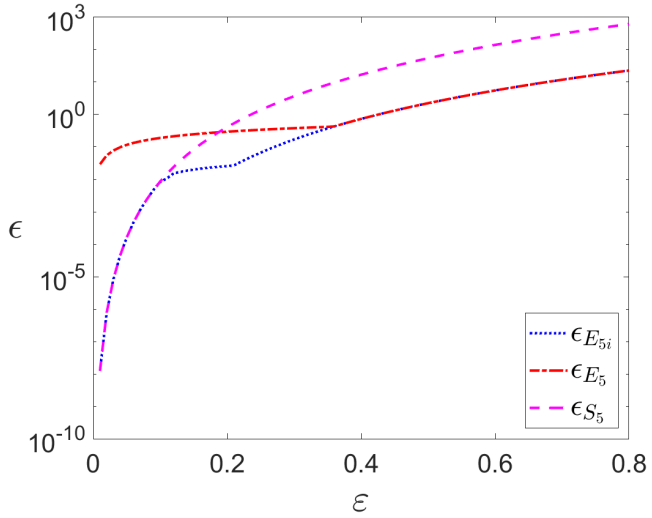


FIG. 6. Absolute relative errors as percentages of the approximate solutions on a semilogarithmic scale, for the in-phase configuration. Here ϵ_{S_5} (magenta, dashed), ϵ_{E_5} (red, dash-dotted) and $\epsilon_{E_{5i}}$ (blue, dotted) denote the errors of the standard series S_5, the Euler E_5 and the improved Euler E_{5i} approximations, respectively, with respect to the numerical solution.

so that the anti-continuum limit is the trivially localized configuration $\{\ldots, 0, 0, 1, -1, 0, 0, \ldots\}$. Proceeding as before for $n = 5$, we obtain

$$\begin{aligned} v_0 &\simeq 1 + \frac{3\varepsilon}{2} - \frac{13\varepsilon^2}{8} + \frac{55\varepsilon^3}{16} - \frac{1213\varepsilon^4}{128} + \frac{7501\varepsilon^5}{256} & v_3 &\simeq \varepsilon^3 - \frac{9\varepsilon^4}{2} + \frac{139\varepsilon^5}{8}, \\ v_1 &\simeq \varepsilon - \frac{\varepsilon^2}{2} + \frac{11\varepsilon^3}{8} - \frac{53\varepsilon^4}{16} + \frac{1203\varepsilon^5}{128} & v_4 &\simeq \varepsilon^4 - \frac{13\varepsilon^5}{2}, \\ v_2 &\simeq \varepsilon^2 - \frac{5\varepsilon^3}{2} + \frac{59\varepsilon^4}{8} - \frac{361\varepsilon^5}{16} & v_5 &\simeq \varepsilon^5. \end{aligned} \tag{11}$$

The corresponding transformed expansions are provided in the supplementary material of this manuscript. This configuration is a two-site state (at the AC limit) where half of the right part of the lattice moves in opposition with the left one. In this case we chose not to present portrait figures to avoid repetition since the findings are quite similar to the ones shown in Figs.4–5. The associated percentage absolute relative errors are shown in Fig. 7. Once more the improved Euler approximation interpolates between S_5 at small ε and E_5 at large ε, and is the most accurate of the three over the whole range of ε considered. Note that the calculations here have been done up to $\varepsilon \simeq 0.77$ due to the specific range of existence of the solution in the out-of-phase configuration. At this specific coupling value, the linear spectrum reaches 0 and the localized solution is terminated by bifurcating to a non-localized one.

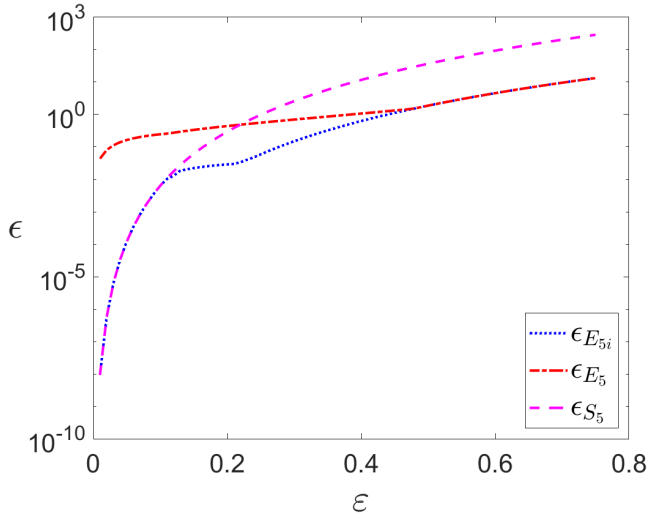


FIG. 7. Absolute relative errors as percentages of the approximate solutions on a semilogarithmic scale, for the out-of-phase configuration. Here ϵ_{S_5} (magenta,dashed), ϵ_{E_5} (red,dash-dotted) and $\epsilon_{E_{5i}}$ (blue,dotted) denote the errors of the standard series S_5, the Euler E_5 and the improved Euler E_{5i} approximations, respectively, with respect to the numerical solution.

It is worth explaining why convergence acceleration is needed in the first place. We have computed the expansion of ν_0 to order 34 (results not shown) and examined the ratios of successive coefficients. For all three configurations, these ratios remain bounded, with

$$3.6 \lesssim \left| \frac{\nu_0^{(k)}}{\nu_0^{(k-1)}} \right| \lesssim 5.1,$$

rather than exhibiting the approximately linear growth with k characteristic of factorially divergent asymptotic expansions. Although finite-order calculations cannot establish convergence, the observed behavior strongly suggests that the expansions have a finite, nonzero estimated radius of convergence of order $\epsilon_c \simeq 0.2$. As ϵ approaches this value, successive terms cease to decrease rapidly, so a truncation after only five terms becomes increasingly inaccurate. This is consistent with the deterioration of the S_5 approximation observed in Figs. 3–7, and motivates the use of the Euler transformation.

IV. STABILITY OF THE TWO-SITE CONFIGURATIONS

As a measure of the agreement of our approximations we now examine the linear stability of the computed solutions, which is determined by the eigenvalues of the stability matrix of the cubic DNLS equation (see e.g. Ref. [5]§2.1),

$$J = \begin{pmatrix} 0 & A_1 \\ A_2 & 0 \end{pmatrix}, \tag{12}$$

where, for a lattice of sites $j, k = -M, \ldots, M$, the two blocks are the tridiagonal matrices

$$(A_1)_{jk} = \left(1 + 2\varepsilon - v_j^2\right) \delta_{jk} - \varepsilon \left(\delta_{j,k+1} + \delta_{j,k-1}\right), \qquad (A_2)_{jk} = -\left(1 + 2\varepsilon - 3v_j^2\right) \delta_{jk} + \varepsilon \left(\delta_{j,k+1} + \delta_{j,k-1}\right), \tag{13}$$

for the real waveforms considered herein, with δ_{jk} the Kronecker delta.

As is discussed, e.g., in [5], the single site configuration is not relevant to consider in the vicinity of the AC limit (but rather only in the vicinity of the continuum one), as there are no nonzero eigenvalues that are bifurcating from the origin of the spectral plane, i.e., $\lambda = 0$. Hence, we focus on the in-phase and out-of-phase two-site configurations.

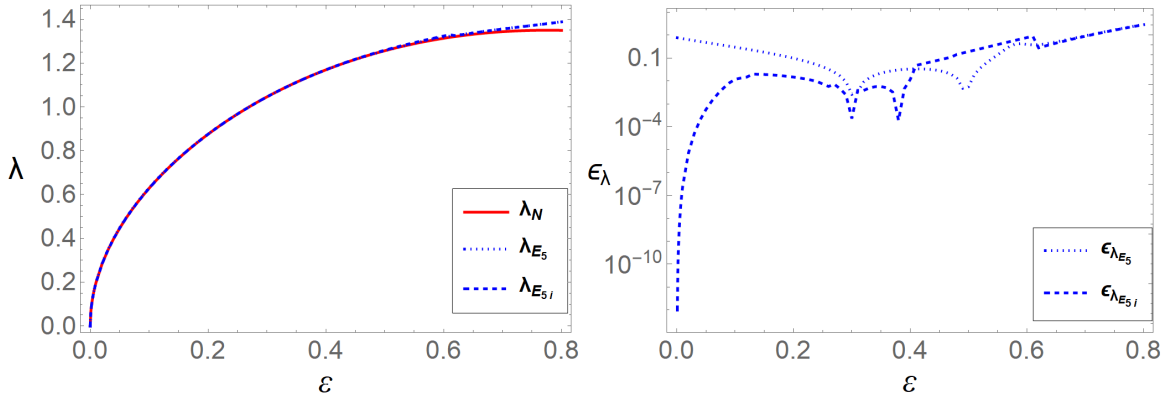


FIG. 8. Comparison between the standard λ_{E_5} (Blue, dotted)- and the improved-Euler $\lambda_{E_{5i}}$ (Blue, dashed), obtained by the semi-numerical method described in the text, with the numerical λ_N (red, solid) unstable (real) eigenvalue for the in-phase case. The left panel shows an excellent agreement between all curves, which is confirmed by the relative errors $\epsilon_{\lambda_{E_5}}$ and $\epsilon_{\lambda_{E_{5i}}}$, plotted on a semilogarithmic scale in the right panel.

A. The in-phase configuration

As shown in Ref. [12], in the in-phase two-site case the linear spectrum of the discrete-soliton solution lies on the imaginary axis in two conjugate bands, while a pair of eigenvalues remains at zero, as is standard for a standing wave in the DNLS model (which enjoys the so-called phase or gauge invariance associated with the conservation of the l^2 norm). In addition, an isolated pair of opposite eigenvalues $(\lambda, -\lambda)$ appears on the real axis, the positive member of which renders the solution unstable. To leading order this unstable eigenvalue was found in Ref. [12] to be $\lambda^{(1/2)} = 2\sqrt{\varepsilon}$, where the superscript records the highest power of ε retained.

We wish to calculate the unstable eigenvalue by using a semi-numerical approach and the improved Euler E_{5i} approximation of this configuration. The full transformation is presented in the supplementary material of this manuscript. To this end, the numerical values of the transformed solutions are substituted into the stability matrix for each $\varepsilon \in [0, 0.8]$, and the corresponding eigenvalue, denoted by $\lambda_{E_{5i}}$, is computed. Then we repeat the procedure in order to calculate the same eigenvalue but by using the E_5 approximation. We call this eigenvalue λ_{E_5}. The results are shown in the left panel of Figure 8, where these eigenvalues are depicted together with λ_N which is the eigenvalue obtained from the fully numerical solution. The curves are almost indistinguishable up to $\varepsilon = 0.6$ while they are still really close up to $\varepsilon = 0.8$. To examine the difference more closely we compute the absolute relative error of λ_{E_5} and $\lambda_{E_{5i}}$, taking λ_N as the reference value. The error for λ_{E_5} is defined as

$$\epsilon_{\lambda_{E_5}} = 100\,\frac{|\lambda_{E_5} - \lambda_N|}{|\lambda_N|}, \tag{14}$$

while $\epsilon_{\lambda_{E_{5i}}}$ is defined similarly. The result is shown in the right panel of Fig. 8. As we can see the error remains below 1% even for $\varepsilon = 0.7$. We can see again that the E_{5i} solution provides better results for small ε but in general, as we mentioned also in the solution section, the standard Euler transform is adequate for most uses while the improved one is useful if fine tuning is needed.

Although the procedure above delivers the unstable eigenvalue, it does not provide a closed-form expression for it as a function of the coupling parameter, of the kind obtained in Ref. [12]. We therefore turn to an asymptotic expansion of the unstable eigenvalue in powers of ε, with the aim of deriving a more tractable analytical approximation.

Following a procedure analogous to the one described in the previous section, we compute the approximate solutions S_n for $n = 1, \ldots, 5$, insert them into the stability matrix and evaluate the corresponding unstable eigenvalue analytically up to order $\varepsilon^{9/2}$ using MATHEMATICA. The results are collected in Table II.

Table II shows clearly how the coefficients of the eigenvalue expansion stabilize as the order of the solution increases. The leading-order result $\lambda^{(1/2)} = 2\varepsilon^{1/2}$ of Ref. [12] is already recovered from the first-order approximation of the solution. The coefficient of the $\varepsilon^{5/2}$ term stabilizes at the level of the S_3 approximation, giving $\lambda^{(5/2)} = 2\varepsilon^{1/2} - \varepsilon^{5/2}$, while the coefficient of the $\varepsilon^{7/2}$ term requires the S_4 solution and yields $\lambda^{(7/2)} = 2\varepsilon^{1/2} - \varepsilon^{5/2} - 4\varepsilon^{7/2}$. These approximations are compared with the numerical eigenvalue λ_N in Fig. 9. The $\lambda^{(5/2)}$ approximation is clearly the closest

S_n	Unstable eigenvalue
S_1	$\sqrt{\varepsilon}\left(2-\frac{5}{8}\varepsilon+\frac{455}{256}\varepsilon^2-\frac{38877}{4096}\varepsilon^3+\frac{19659275}{262144}\varepsilon^4\right)$
S_2	$\sqrt{\varepsilon}\left(2+\frac{5}{16}\varepsilon^2-\frac{1425}{128}\varepsilon^3+\frac{80639}{1024}\varepsilon^4\right)$
S_3	$\sqrt{\varepsilon}\left(2-\varepsilon^2-\frac{1005}{128}\varepsilon^3+\frac{661}{8}\varepsilon^4\right)$
S_4	$\sqrt{\varepsilon}\left(2-\varepsilon^2-4\varepsilon^3+\frac{18687}{256}\varepsilon^4\right)$
S_5	$\sqrt{\varepsilon}\left(2-\varepsilon^2-4\varepsilon^3+\frac{239}{4}\varepsilon^4\right)$

TABLE II. The unstable eigenvalue of the in-phase configuration, obtained from the solution approximations S_1 through S_5.

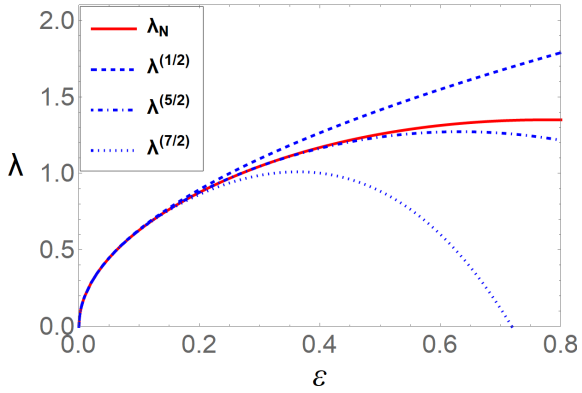


FIG. 9. Comparison of the asymptotic approximations of the unstable eigenvalue in the in-phase case, $\lambda^{(1/2)}$ (blue, dashed), $\lambda^{(5/2)}$ (blue, dash-dotted) and $\lambda^{(7/2)}$ (blue, dotted), with the numerical eigenvalue λ_N (red,solid). The $\lambda^{(5/2)}$ approximation provides the best agreement with the numerical result.

to the numerical result; including the next term, of order $\varepsilon^{7/2}$, makes the approximation worse and causes it to deviate from λ_N. This behaviour is characteristic of an asymptotic rather than a convergent expansion: the optimal truncation is attained at order $\varepsilon^{5/2}$, beyond which further terms degrade the approximation.

Finally, we apply the standard Euler transform E_5 to the S_5 solution, insert the transformed profile into the stability matrix and obtain, up to $\mathcal{O}(\varepsilon^{5/2})$, the approximation

$$\lambda_{E_5}^{(5/2)}=\frac{\sqrt{\varepsilon}}{\sqrt{65}}\left(\frac{65}{4}-\frac{1287}{1024}\varepsilon-\frac{1955013}{2621440}\varepsilon^2\right).$$

This approximation is shown together with $\lambda_{E_{5i}}$, $\lambda^{(5/2)}$ and λ_N in the left panel of Fig. 10, while the right panel displays the corresponding relative errors with respect to the numerical eigenvalue on a semilogarithmic scale.

The improved Euler transform provides the best agreement with the numerical solution, at the cost of a comparatively cumbersome implementation and without providing an analytic formula. The $\lambda^{(5/2)}$ approximation, although less accurate, offers a considerably simpler closed-form expression and may therefore be preferable whenever high accuracy is not

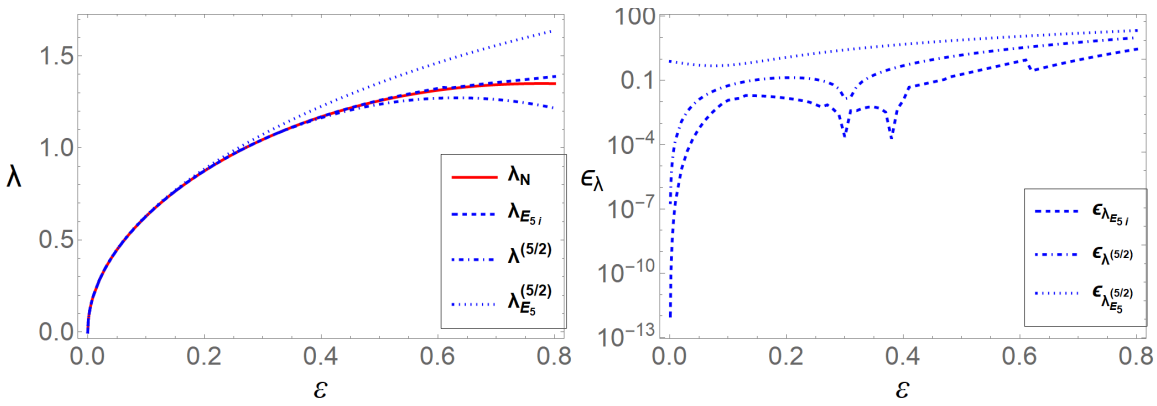


FIG. 10. The unstable eigenvalue of the in-phase configuration. The left panel compares the numerical eigenvalue λ_N (red,solid), the optimal truncation $\lambda^{(5/2)}$ (blue, dash-dotted), the result $\lambda^{(5/2)}_{E_5}$ (blue, dotted) obtained with the standard Euler transform and truncated to terms up to $\varepsilon^{5/2}$, and the result $\lambda_{E_{5i}}$ (blue, dashed) obtained from the semi-numerical use of the improved Euler transform. The right panel shows the relative error of each approximation with respect to the numerical eigenvalue.

required. It is an intriguing observation (for which we have no intuitive explanation) that the error of $\lambda^{(5/2)}$ is smaller than $\lambda^{(5/2)}_{E_5}$.

B. The out-of-phase configuration

In this case, it was already established in [12] that an isolated pair of eigenvalues also exists yet in this case it lies on the imaginary axis for sufficiently small ε. Accordingly, the configuration is spectrally stable until the pair collides with the linear spectrum and the solution is destabilized through a Hamiltonian–Hopf bifurcation. However, it is still instructive to track the relevant eigenvalues, both as a further test of our approach and in order to see whether the estimate of Ref. [12] can be improved. We therefore repeat the procedure of the previous subsection: The full improved Euler transformation E_{5i} is calculated (and presented as supplementary material of the manuscript). Then, the corresponding transformed solutions are evaluated numerically for each $\varepsilon \in [0, 0.6]$, inserted into the stability matrix (12)–(13), and the isolated eigenvalue with positive imaginary part is computed. We do not pursue larger values of ε, since there are several bifurcations occurring rendering the results irrelevant as we are going to see in what follows.

The results are shown in the left panel of Fig. 11, where the imaginary part of the λ_{E_5} and $\lambda_{E_{5i}}$ eigenvalues is compared with its fully numerical counterpart λ_N. The agreement between the curves is adequate, but neither as close nor as smooth as in the in-phase configuration (cf. Fig. 8). The reason is that here the isolated eigenvalue collides with the linear spectrum, giving rise to a complex quartet [12], and consequently the "interaction" between the relevant eigenvalues affects such collisions and the resulting eigenvalue dependencies. For the fully numerical eigenvalue this happens only once, at $\varepsilon \simeq 0.146$, producing a single spike in the $\lambda(\varepsilon)$ curve: on a sufficiently large lattice the complex pair cannot re-enter the imaginary axis before it reaches the end of the linear spectrum. The series approximations, by contrast, have only 12 non-zero sites, so that the corresponding stability matrix is 24×24 and possesses only 10 eigenvalues with positive imaginary part. There is consequently ample room on the imaginary axis for the complex pair to leave and re-enter repeatedly, which produces the succession of "corners" visible in $\lambda_{E_{5i}}(\varepsilon)$. We emphasize that this is an artifact of the finite truncation of the series solution, not of the acceleration procedure itself. The right panel of the same figure shows the errors $\epsilon_{\lambda_{E_5}}$ and $\epsilon_{\lambda_{E_{5i}}}$ defined in Eq. (14). Several spikes are visible, caused both by the collisions described above and by the switching between the branches of the improved Euler transformation, but the error nevertheless remains of the order of 1%. At this point one could also be tempted to compare the real part of the eigenvalues as well. However, this is not very meaningful due to the many departures and re-entrances of the eigenvalue from the imaginary axis as described above. On the other hand, it is interesting to observe that this semi-numerical approach is very accurate. Remarkably, it reveals rather accurately the bifurcation point in which the linearly stable solution becomes unstable.

As before, since this semi-numerical approach does not yield a single closed-form expression for the eigenvalue, we return to the standard series solution and seek an asymptotic expansion. We substitute the approximate solutions S_1 through S_5 into the stability matrix and compute analytically the eigenvalue using MATHEMATICA; the resulting

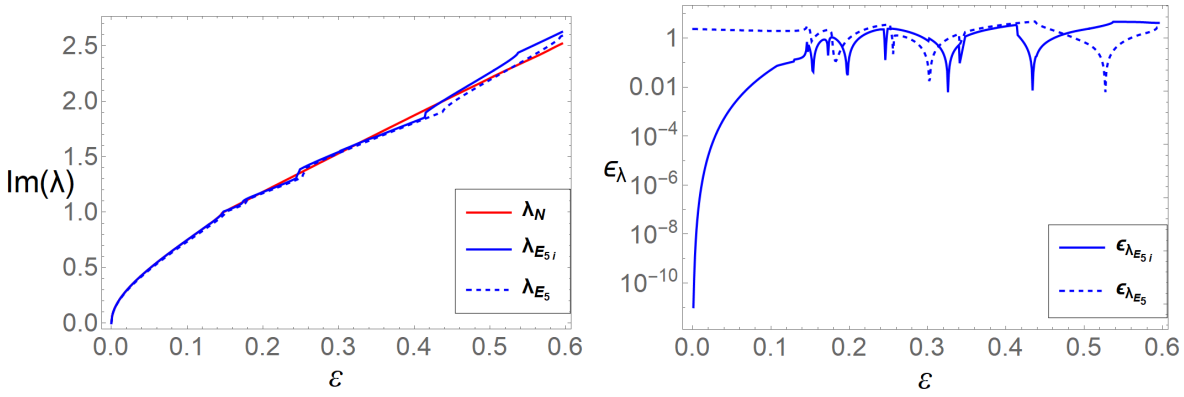


FIG. 11. The out-of-phase configuration. The left panel shows λ_{E_5} (blue, dashed) and $\lambda_{E_{5i}}$ (blue,solid), obtained by the semi-numerical method described in the text, together with λ_N (red,solid), while the right panel shows the corresponding relative error $\epsilon_{\lambda_{E_5}}$ and $\epsilon_{\lambda_{E_{5i}}}$.

eigenvalues are listed in Table III.

S_n	Eigenvalue
S_1	$\mathrm{i}\sqrt{\varepsilon}\left(2+\frac{45}{8}\varepsilon+\frac{375}{256}\varepsilon^2+\frac{23253}{4096}\varepsilon^3+\frac{5045483}{262144}\varepsilon^4\right)$
S_2	$\mathrm{i}\sqrt{\varepsilon}\left(2+4\varepsilon-\frac{135}{16}\varepsilon^2+\frac{657}{128}\varepsilon^3+\frac{8311}{1024}\varepsilon^4\right)$
S_3	$\mathrm{i}\sqrt{\varepsilon}\left(2+4\varepsilon-5\varepsilon^2+\frac{3517}{128}\varepsilon^3+\frac{131}{64}\varepsilon^4\right)$
S_4	$\mathrm{i}\sqrt{\varepsilon}\left(2+4\varepsilon-5\varepsilon^2+18\varepsilon^3-\frac{15245}{256}\varepsilon^4\right)$
S_5	$\mathrm{i}\sqrt{\varepsilon}\left(2+4\varepsilon-5\varepsilon^2+18\varepsilon^3-\frac{121}{4}\varepsilon^4\right)$

TABLE III. The isolated eigenvalue of the out-of-phase configuration, obtained from the solution approximations S_1 through S_5.

Here too the coefficients of the eigenvalue expansion converge as the degree of the solution increases. From the table we obtain the $\mathcal{O}(\varepsilon^{1/2})$, $\mathcal{O}(\varepsilon^{3/2})$, $\mathcal{O}(\varepsilon^{5/2})$ and $\mathcal{O}(\varepsilon^{7/2})$ truncated approximations of the imaginary part of the isolated eigenvalue, namely $\lambda^{(1/2)}=2\varepsilon^{1/2}$, $\lambda^{(3/2)}=2\varepsilon^{1/2}+4\varepsilon^{3/2}$, $\lambda^{(5/2)}=2\varepsilon^{1/2}+4\varepsilon^{3/2}-5\varepsilon^{5/2}$ and $\lambda^{(7/2)}=2\varepsilon^{1/2}+4\varepsilon^{3/2}-5\varepsilon^{5/2}+18\varepsilon^{7/2}$, respectively. These are shown together with the numerical eigenvalue λ_N in Fig. 12; $\lambda^{(1/2)}$ is the estimate reported in Ref. [12]. The $\lambda^{(3/2)}$ approximation already captures the main behaviour of the numerical eigenvalue, and the inclusion of the next term in $\lambda^{(5/2)}$ leads to a noticeably better agreement. Incorporating the subsequent $\varepsilon^{7/2}$ contribution in $\lambda^{(7/2)}$, on the other hand, does not improve matters; the resulting curve diverges from the numerical eigenvalue faster than any of the others. As in the in-phase case, this progressive deterioration is the signature of an asymptotic expansion, and $\lambda^{(5/2)}$ is again the optimal truncation.

Finally, applying the standard Euler transform E_5 to the S_5 solution and inserting the transformed profile into the

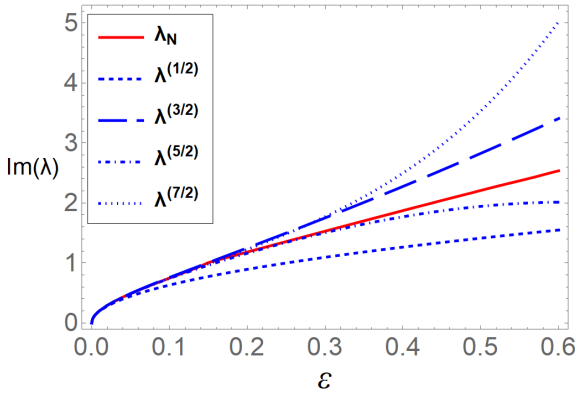


FIG. 12. Comparison between the numerical eigenvalue λ_N (red,solid) and the asymptotic approximations $\lambda^{(1/2)}$ (blue, dashed), $\lambda^{(3/2)}$ (blue, long-dashed), $\lambda^{(5/2)}$ (blue, dash-dotted) and $\lambda^{(7/2)}$ (blue, dotted) defined in the text, for the out-of-phase configuration. The $\lambda^{(5/2)}$ approximation is the closest to the numerical result.

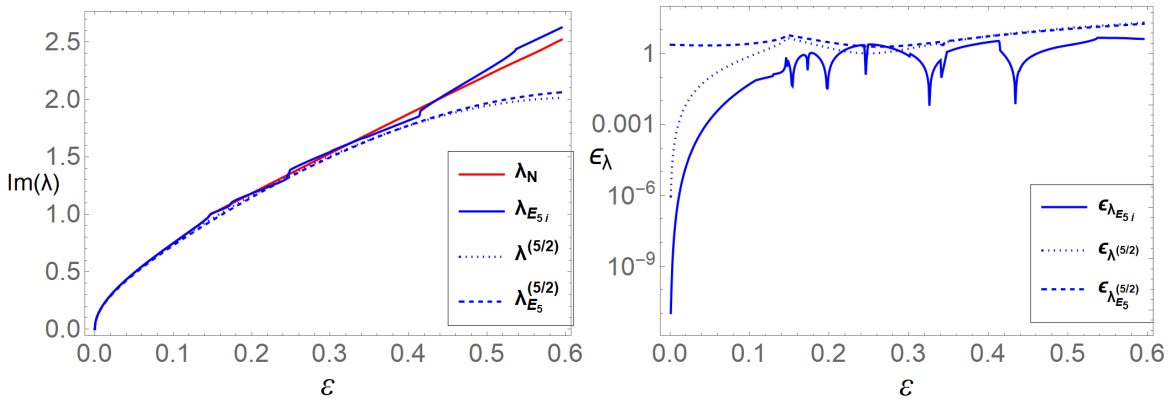


FIG. 13. Comparison of the positive imaginary part of the isolated eigenvalue of the out-of-phase configuration, as obtained from the numerical solution λ_N (red,solid), from the improved Euler transform $\lambda_{E_{5i}}$ (blue,solid), from the series expansion truncated at the $\varepsilon^{5/2}$ term $\lambda^{(5/2)}$ (blue, dotted), and from the standard Euler transform $\lambda_{E_5}^{(5/2)}$ (blue,dashed) (left panel). The corresponding relative errors with respect to the numerical eigenvalue are shown in the right panel.

stability matrix gives, up to $\mathcal{O}(\varepsilon^{5/2})$,

$$\lambda_{E_5}^{5/2} = \frac{i\sqrt{\varepsilon}}{\sqrt{61}}\left(\frac{61}{4} + \frac{32063}{1024}\varepsilon - \frac{1174093393}{31981568}\varepsilon^2\right).$$

This approximation is shown together with $\lambda_{E_{5i}}$, $\lambda^{(5/2)}$ and λ_N in Fig. 13, whose right panel again displays the corresponding relative errors with respect to the numerical eigenvalue on a semilogarithmic scale. Once again, $\lambda^{(5/2)}$ provides a reasonable approximation over a wide range of ε values.

V. CONCLUSIONS AND FUTURE DIRECTIONS

In this paper we constructed approximate discrete-soliton solutions of the cubic discrete nonlinear Schrödinger equation, for which exact analytical solutions are not available. Yet, the model is one of wide physical applicability in systems ranging from arrays of optical waveguides [3, 5] to optical lattices of atomic condensates (with the latter also becoming more experimentally accessible recently [39]). Three configurations were considered: the standard single-site one and the two two-site ones, in-phase and out-of-phase. The standard perturbation method delivers sign-alternating series expansions, which makes the Euler transform, in both its standard and its improved form, a natural tool for the acceleration

of the convergence of the solution. Both transformations improved the accuracy of the solution appreciably and, importantly, helped to preserve its exponentially localized character over a substantially wider range of couplings. It is worth emphasizing how the improved transformation interpolates automatically between the plain series at small ε and the standard Euler transform at large ε, selecting in each case the better one among the two. If such fine tuning is unnecessary, the standard transform provides adequate accuracy with a simpler, more standard algorithm.

As a benchmark of our approach we then characterized the stability of these solutions through the eigenvalues of the stability matrix. Since the single-site configuration is spectrally stable throughout the range considered, and therefore of no interest in this respect, we concentrated on the two-site configurations. For the in-phase configuration we focused on the real, positive (unstable) eigenvalue. A semi-numerical approach, in which the standard and improved-Euler profiles are evaluated and inserted into the stability matrix, reproduces the fully numerical eigenvalue to better than 1% up to $\varepsilon = 0.7$. Going further, we asked whether our approach could improve on the leading-order estimate $2\sqrt{\varepsilon}$ of Ref. [12]. Examining the successive truncations, we concluded that the $\mathcal{O}(\varepsilon^{5/2})$ result derived from the standard series solution, $\lambda^{(5/2)} = 2\varepsilon^{1/2} - \varepsilon^{5/2}$, agrees best with the numerical eigenvalue and constitutes a significant improvement on the previously available eigenvalue estimate; here the Euler transformation offers no further gain. In addition, we also examined the isolated eigenvalue of the out-of-phase configuration, as an additional test of the method. The results parallel those of the in-phase case, with the added richness — and the added difficulty for the semi-numerical approach — caused by the collisions of the isolated eigenvalue with the continuous spectrum, which on the truncated lattice occur repeatedly rather than once. Despite the limitations (e.g., as concerns the real part of the approximation), the methodology provides a reasonable (and far more widely applicable than previously available) estimate of the next order correction approximation of the solutions' eigenvalues.

Overall, the Euler transform provides reasonably accurate analytical approximations of discrete-soliton solutions while the use of the series solutions acquired by standard perturbation theory improves the analytical stability estimates available so far. Finally, the semi-numerical variant of the approach reproduces the eigenvalue of interest to remarkable accuracy. Two limitations should be kept in mind: the accuracy attainable is ultimately bounded by the optimal truncation of an asymptotic expansion, and the number of non-zero sites retained by a fifth-order expansion is what generates the spurious eigenvalue collisions observed in the out-of-phase case. One can mitigate this issue by considering a larger number of non-zero sites, at the potential additional expense of more cumbersome expressions.

Although the linear Euler transformation already yields significant improvements, a natural extension of this study would be to consider nonlinear resummation techniques such as the Padé and Shanks transformations [27, 28, 33, 36], which are not restricted to sign-alternating series and which we expect to improve the results further and to provide additional insight into the system under consideration. Furthermore, while in the present study we restricted consideration to one-dimensional configurations, a natural question arises as to the applicability of such techniques to more elaborate (yet still experimentally attainable [40, 41]) configurations such as discrete vortices in two-dimensional settings [13] and perhaps even their more exotic extensions in three spatial dimensions [14]. Such studies are currently in progress and will be reported in future publications.

[1] M. J. Ablowitz, *Nonlinear Dispersive Waves: Asymptotic Analysis and Solitons* (Cambridge University Press, 2011).
[2] A. Scott, *Nonlinear Science: Emergence and Dynamics of Coherent Structures*, 2nd ed. (Oxford University Press, Oxford, 2003).
[3] M. J. Ablowitz, B. Prinari, and A. D. Trubatch, *Discrete and Continuous Nonlinear Schrödinger Systems* (Cambridge University Press, Cambridge, 2004).
[4] T. Dauxois and M. Peyrard, *Physics of Solitons* (Cambridge University Press, Cambridge, 2006).
[5] P. G. Kevrekidis, *The Discrete Nonlinear Schrödinger Equation: Mathematical Analysis, Numerical Computations and Physical Perspectives*, Springer Tracts in Modern Physics, Vol. 232 (Springer, Berlin, Heidelberg, 2009).
[6] P. G. Kevrekidis, D. J. Frantzeskakis, and R. Carretero-González, *The Defocusing Nonlinear Schrödinger Equation: From Dark Solitons to Vortices and Vortex Rings* (SIAM, Philadelphia, 2015).
[7] R. S. MacKay and S. Aubry, Nonlinearity **7**, 1623 (1994).
[8] S. Flach and C. R. Willis, Physics Reports **295**, 181 (1998).
[9] S. Flach and A. V. Gorbach, Physics Reports **467**, 1 (2008).
[10] S. Aubry, Physica D **103**, 201 (1997).
[11] S. Aubry, Physica D **216**, 1 (2006).
[12] D. E. Pelinovsky, P. G. Kevrekidis, and D. J. Frantzeskakis, Physica D **212**, 1 (2005).
[13] D. E. Pelinovsky, P. G. Kevrekidis, and D. J. Frantzeskakis, Physica D **212**, 20 (2005).
[14] M. Lukas, D. Pelinovsky, and P. Kevrekidis, Physica D: Nonlinear Phenomena **237**, 339 (2008).
[15] D. E. Pelinovsky and A. Sakovich, Physica D **240**, 265 (2011).

[16] J. Archilla, J. Cuevas, B. Sánchez-Rey, and A. Alvarez, Physica D: Nonlinear Phenomena **180**, 235 (2003).
[17] V. Koukouloyannis and P. G. Kevrekidis, Nonlinearity **22**, 2269 (2009).
[18] T. Ahn, R. S. MacKay, and J.-A. Sepulchre, Nonlinear Dynamics **25**, 157 (2001).
[19] V. Koukouloyannis and R. S. MacKay, Journal of Physics A: Mathematical and General **38**, 1021 – 1030 (2005), cited by: 24.
[20] J. Cuevas-Maraver, V. Koukouloyannis, P. G. Kevrekidis, and J. F. R. Archilla, International Journal of Bifurcation and Chaos **21**, 2161 (2011).
[21] V. Koukouloyannis, P. G. Kevrekidis, J. Cuevas, and V. Rothos, Physica D **242**, 16 (2013).
[22] D. E. Pelinovsky and A. Sakovich, Nonlinearity **25**, 3423 (2012).
[23] J. Cuevas, G. James, P. G. Kevrekidis, B. A. Malomed, and B. Sánchez-Rey, Journal of Nonlinear Mathematical Physics **15**, 124 (2008).
[24] C. M. Bender and S. A. Orszag, *Advanced Mathematical Methods for Scientists and Engineers I: Asymptotic Methods and Perturbation Theory* (Springer, New York, 1999).
[25] G. H. Hardy, *Divergent Series* (Oxford University Press, Oxford, 1949).
[26] É. Borel, Annales scientifiques de l'École Normale Supérieure **16**, 9 (1899).
[27] H. Padé, Annales scientifiques de l'École Normale Supérieure **9**, 3 (1892).
[28] D. Shanks, Journal of Mathematics and Physics **34**, 1 (1955).
[29] P. Wynn, Mathematical Tables and Other Aids to Computation **10**, 91 (1956).
[30] A. van Wijngaarden, in *Cursus: Wetenschappelijk rekenen B: Onderdeel "Proces Analyse"* (Stichting Mathematisch Centrum, Amsterdam, 1965).
[31] D. Levin, International Journal of Computer Mathematics **3**, 371 (1973).
[32] E. J. Weniger, Computer Physics Reports **10**, 189 (1989).
[33] G. A. Baker, Jr. and P. Graves-Morris, *Padé Approximants*, 2nd ed., Encyclopedia of Mathematics and its Applications, Vol. 59 (Cambridge University Press, Cambridge, 1996).
[34] C. Brezinski and M. Redivo Zaglia, *Extrapolation Methods: Theory and Practice*, Studies in Computational Mathematics, Vol. 2 (North-Holland, Amsterdam, 1991).
[35] A. Sidi, *Practical Extrapolation Methods: Theory and Applications*, Cambridge Monographs on Applied and Computational Mathematics, Vol. 10 (Cambridge University Press, Cambridge, 2003).
[36] K. D. Housiadas, Journal of Non-Newtonian Fluid Mechanics **247**, 1 – 14 (2017).
[37] M. Abramowitz and I. A. Stegun, eds., *Handbook of mathematical functions with formulas, graphs, and mathematical tables* (Dover Publications, 1965).
[38] A. van Wijngaarden, *Proces Analyse*, Cursus: Wetenschappelijk Rekenen B (Stichting Mathematisch Centrum, Amsterdam, 1965) mathematisch Centrum, Amsterdam.
[39] R. Cruickshank, F. Lorenzi, A. La Rooij, E. F. Kerr, T. Hilker, S. Kuhr, L. Salasnich, and E. Haller, Phys. Rev. Lett. **135**, 263404 (2025).
[40] D. N. Neshev, T. J. Alexander, E. A. Ostrovskaya, Y. S. Kivshar, H. Martin, I. Makasyuk, and Z. Chen, Phys. Rev. Lett. **92**, 123903 (2004).
[41] J. W. Fleischer, G. Bartal, O. Cohen, O. Manela, M. Segev, J. Hudock, and D. N. Christodoulides, Phys. Rev. Lett. **92**, 123904 (2004).
[42] F. Lederer, G. I. Stegeman, D. N. Christodoulides, G. Assanto, M. Segev, and Y. Silberberg, Phys. Rep. **463**, 1 (2008).
[43] O. Morsch and M. Oberthaler, Rev. Mod. Phys. **78**, 179 (2006).
[44] V. Vulić, N. Šantić, H. Buljan, and D. Aumiler, Laser Photonics Rev. e71994 (2026).

Appendix A: Euler transform: single-site configuration

In this appendix we present the full transformed solution for the single-site configuration, obtained with the improved Euler transformation according to the algorithm of Sec. II.

Throughout the appendix, $\mathcal{S}_n$ denotes the result of the standard perturbation method for a single site of the lattice, the subscript n being the number of terms retained. By $\mathcal{E}_n$ we denote the truncated series obtained after applying the standard Euler transform to $\mathcal{S}_n$, and by $\mathcal{E}^m_{ni}$ the improved Euler transform acting on $\mathcal{S}_n$, with the subscript "i" standing for "improved" and the superscript m labelling which of the n possible series, according to the conditions of Table I, is selected for the given value of ε.

These tables confirm what was observed in Fig. 3: the improved Euler algorithm always selects the series with the smaller error. For small ε the improved transform $\mathcal{E}^n_{ni}$ coincides with the original series $\mathcal{S}_n$, whereas for large ε it becomes the standard Euler transform, $\mathcal{E}^1_{ni} = \mathcal{E}_n$. Note that the branch intervals are in general unions of disjoint sub-intervals, i.e. the algorithm switches back and forth between branches as ε increases; this is the origin of the spikes observed in Figs. 10, 11 and 13. The interval endpoints below are quoted to two decimal places because they were obtained on a grid of $\Delta\varepsilon = 0.01$ and they are not the exact endpoints which correspond to the satisfaction of the conditions of section II.

Oscillator	ε	Transformed series
v_0	$[0, 0.09]$	$\mathcal{S}_5 = \mathcal{E}_{5i}^5 = 1 + \varepsilon - \frac{3\varepsilon^2}{2} + \frac{7\varepsilon^3}{2} - \frac{85\varepsilon^4}{8} + \frac{287\varepsilon^5}{8}$
	$[0.1, 0.11] \cup [0.28, 0.31]$	$\mathcal{E}_{5i}^4 = 1 + \varepsilon - \frac{3\varepsilon^2}{2} + \frac{7\varepsilon^3}{2} - \frac{255\varepsilon^4}{32} + \frac{287\varepsilon^5}{32}$
	$[0.12, 0.27] \cup [0.32, 0.37]$	$\mathcal{E}_{5i}^3 = 1 + \varepsilon - \frac{3\varepsilon^2}{2} + \frac{49\varepsilon^3}{16} - \frac{85\varepsilon^4}{16} + \frac{287\varepsilon^5}{64}$
	$[0.38, 0.53]$	$\mathcal{E}_{5i}^2 = 1 + \varepsilon - \frac{45\varepsilon^2}{32} + \frac{77\varepsilon^3}{32} - \frac{425\varepsilon^4}{128} + \frac{287\varepsilon^5}{128}$
	$[0.54, 1]$	$\mathcal{E}_5 = \mathcal{E}_{5i}^1 = 1 + \frac{31\varepsilon}{32} - \frac{39\varepsilon^2}{32} + \frac{7\varepsilon^3}{4} - \frac{255\varepsilon^4}{128} + \frac{287\varepsilon^5}{256}$
v_1	$[0, 0.1]$	$\mathcal{S}_5 = \mathcal{E}_{5i}^5 = \varepsilon - \varepsilon^2 + \frac{5\varepsilon^3}{2} - \frac{15\varepsilon^4}{2} + \frac{195\varepsilon^5}{8}$
	$\{0.11\} \cup [0.3, 0.32]$	$\mathcal{E}_{5i}^4 = \varepsilon - \varepsilon^2 + \frac{5\varepsilon^3}{2} - \frac{45\varepsilon^4}{8} + \frac{195\varepsilon^5}{32}$
	$[0.12, 0.29] \cup [0.33, 0.36]$	$\mathcal{E}_{5i}^3 = \varepsilon - \varepsilon^2 + \frac{35\varepsilon^3}{16} - \frac{15\varepsilon^4}{4} + \frac{195\varepsilon^5}{64}$
	$[0.37, 0.63]$	$\mathcal{E}_{5i}^2 = \varepsilon - \frac{15\varepsilon^2}{16} + \frac{55\varepsilon^3}{32} - \frac{75\varepsilon^4}{32} + \frac{195\varepsilon^5}{128}$
	$[0.64, 1]$	$\mathcal{E}_5 = \mathcal{E}_{5i}^1 = \frac{31\varepsilon}{32} - \frac{13\varepsilon^2}{16} + \frac{5\varepsilon^3}{4} - \frac{45\varepsilon^4}{32} + \frac{195\varepsilon^5}{256}$
v_2	$[0, 0.1]$	$\mathcal{S}_4 = \mathcal{E}_{4i}^4 = \varepsilon^2 - 3\varepsilon^3 + \frac{19\varepsilon^4}{2} - \frac{63\varepsilon^5}{2}$
	$\{0.11\} \cup [0.31, 0.32]$	$\mathcal{E}_{4i}^2 = \varepsilon^2 - \frac{21\varepsilon^3}{8} + \frac{19\varepsilon^4}{4} - \frac{63\varepsilon^5}{16}$
	$[0.12, 0.3] \cup [0.33, 1]$	$\mathcal{E}_4 = \mathcal{E}_{4i}^1 = \frac{15\varepsilon^2}{16} - \frac{33\varepsilon^3}{16} + \frac{95\varepsilon^4}{32} - \frac{63\varepsilon^5}{32}$
v_3	$[0, 0.06]$	$\mathcal{S}_3 = \mathcal{E}_{3i}^3 = \varepsilon^3 - 5\varepsilon^4 + \frac{41\varepsilon^5}{2}$
	$[0.23, 0.26]$	$\mathcal{E}_{3i}^2 = \varepsilon^3 - \frac{15\varepsilon^4}{4} + \frac{41\varepsilon^5}{8}$
	$[0.07, 0.22] \cup [0.27, 1]$	$\mathcal{E}_3 = \mathcal{E}_{3i}^1 = \frac{7\varepsilon^3}{8} - \frac{5\varepsilon^4}{2} + \frac{41\varepsilon^5}{16}$
v_4	$[0, 0.04]$	$\mathcal{S}_2 = \mathcal{E}_{2i}^2 = \varepsilon^4 - 7\varepsilon^5$
	$[0.05, 1]$	$\mathcal{E}_2 = \mathcal{E}_{2i}^1 = \frac{3\varepsilon^4}{4} - \frac{7\varepsilon^5}{4}$
v_5	$[0, 1]$	$\mathcal{S}_1 = \mathcal{E}_1 = \mathcal{E}_{1i}^1 = \varepsilon^5$

TABLE IV. Transformed series for the single-site configuration, listed by lattice site and by the range of ε over which each branch of the improved Euler transformation is selected.